Available at www.ComputerScienceWeb.com
POWERED BY SCIENCE DIRECT®

Pattern Recognition Letters 24 (2003) 2471–2478

Pattern Recognition Letters

www.elsevier.com/locate/patrec

Automated detection of blood vessels using dynamic programming

Peter J. Yim *, Mark Kayton, Walter Miller, Steven Libutti, Peter L. Choyke

Department of Radiology MEB 404, Robert Wood Johnson Medical School, 1 Robert Wood Johnson Place #357, New Brunswick, NJ 08903, USA

Received 19 December 2002; received in revised form 12 March 2003

Abstract

An essential step in the characterization of angiography is the detection of the blood vessels. We propose an algorithm for detection of vessels in two-dimensional angiography from an acyclic graph that represents optimal paths within the image.

Keywords: Angiography; Detection; Graph representation

1. Introduction

Angiography encompasses a wide spectrum of methodologies for imaging blood vessels for planning and guidance of surgical procedures. Most recently, angiography has been employed on the microscopic scale for the study vascular density and its relation to the process of angiogenesis (Hazel, 2003). Conventional applications of angiography include identification and grading of arterial stenoses (Rothwell et al., 1994) or aneurysms (Brown et al., 2003), identification of arteries that feed arteriovenous malformations (Bullitt et al., 2001). Angiography is usually interpreted visually, however, there are many potential advantages of computational analysis of angiography including increased precision in interpretation and the ability to handle complex tasks such as image fusion for treatment of tumors (Gering et al., 2001) and reconstruction of vascular shape from biplane angiography and intravascular ultrasound (Cothren et al., 2000).

A fundamental component of angiography analysis is vessel detection. Vessel detection is a recognition problem that is challenging due to the complex nature of vascular trees and to imaging imperfections. One inherent imperfection of angiography is the intensity inhomogeneity between the larger and smaller vessels. Another imperfection common to many angiographic methods is the leakage of contrast agent into the background tissue that reduces the contrast between vessels and tissue.

* Corresponding author. Tel.: +1-732-235-8911; fax: +1-732-235-6889.
E-mail address: yimpj@umdnj.edu (P.J. Yim).

0167-8655/03/$ - see front matter © 2003 Published by Elsevier B.V.
doi:10.1016/S0167-8655(03)00092-8

Detection of vessels has been approached both as a segmentation problem (Eichel et al., 1986; Nguyen and Sklansky, 1986; Yim et al., 1998) and as centerline-detection problem. Centerline-detection is advantageous in several respects and is the focus of this paper. Centerline-detection is particularly appropriate for smaller vessels whose most prominent feature is their axial continuity. Moreover, centerlines are a meaningful description of the vessel that can be used as a basis for diameter measurements.

Several methodologies for semi-automated detection of vessel centerlines have been proposed (Sun, 1989; Sen et al., 1999; Aylward, 2002; Merle et al., 1998). Detection of the vessel centerline, in these methodologies, is based on the identification of one or more points along the vessel. The algorithm of Sun (Sun, 1989) tracks vessels in projection angiography by a matched filter. The algorithm incorporates constraints on the continuity of vessel attributes including vessel width, density and directionality. In a similar manner, the set of algorithms proposed by Sen et al. (Sen et al., 1999) track vessels by scanning for points of maximal image-intensity under certain constraints on vessel directionality. Problems with propagation into the fainter distal vessels are addressed in their algorithms by requiring the user to identify a distal point for each vessel segment. The algorithm of Aylward (Aylward, 2002) incorporates a differential geometry model of ridges in images (Eberly et al., 1994). The algorithm detects vessel directionality in an analytic manner from the Hessian matrix for a given point and has been found to be suitable for detection of vessel centerlines in 3D angiography. An algorithm based on a similar model has been proposed by Merle et al. for use in centerline-detection in coronary angiography (Eichel et al., 1986).

All previous algorithms for centerline-detection, to the best of our knowledge, employ local criteria for defining ridge points. Complete centerlines are then assembled by tracking or clustering of potential ridge points. The methods for formation of the centerlines from ridge points, as described above, are reasonable but essentially ad hoc and require tuning of parameters. Most significantly, the above-mentioned centerline-detection algorithms all require assumptions of vessel shape. We propose an alternative approach for vessel detection that is based purely on the image-intensity structure. In this approach all potential vessel paths are extracted from a set of optimal paths represented in an acyclic graph generated by the ordered region growing (ORG) algorithm (Yim et al., 2000 Choyke et al., 2001). Paths within the graph are optimal according to the "greatest-minima" criteria; for any ORG path, the minimum image intensity along that path is greater than or equal to that of any alternate path between the same two endpoints (Yim et al., in press). The acyclic graph is then reduced to true vessel paths in subsequent straight-forward steps. The algorithm does not entirely avoid the necessity of parameter selection. However, primary parameter associated with the proposed algorithm is essentially the confidence level of a statistical test.

The initial motivation for the methodology proposed here is extraction of the vessel axes and measurement of total vessel length in microscopic angiography. This analysis is needed for objective assessment of vascularity for the study of angiogenesis. The methodology may, however, generalize to a wider range of applications in angiography. The ORG algorithm is discussed in detail in the following section.

2. Background: The ORG algorithm

The process of vessel detection is based on a directed acyclic graph generated by the ORG algorithm. Previously, the ORG algorithm was used in a straight-forward manner for semi-automated delineation of vessel paths in 3D angiography. Since the acylic graph generated by the ORG algorithm defines an optimal, unique path between any two points in the image, in principle, any vessel can be delineated by manual identification of the proximal and distal endpoints. This methodology is suitable for 3D angiography where vessel paths are unambiguous and where there may be only a small number of vessels of interest. However, this procedure is not adequate for projection angiography where the path of a given vessel may be ambiguous due to the visual occlu-

sion by other vessels and where there are a large number of vessels of interest. This ambiguity of projection angiography leads to two types of errors for the ORG algorithm. First, overlapping but distinct vessels may be represented as connected paths within the ORG graph or, secondly, a single vessel segment may be a disjoint path in the ORG graph. The latter situation will occur when vessels overlap so as to produce a cyclical structure in the projection image that are disallowed by the ORG algorithm. However, on the whole, even for projection angiography, the ORG produces as graph that is highly inclusive of paths along the vessel axes. Thus, while ORG algorithm cannot be applied directly for vessel detection in projection angiography, the graph generated by the ORG algorithm serves as an excellent basis for a more sophisticated vessel-detection scheme. The proposed algorithm is appropriate for low-level vessel detection and is suitable for measurement of total vessel length, for example. However, this algorithm is not sufficient for defining the correct connectivity amongst vessels in 2D angiography although it might be a good starting point for doing so. In the remainder of this section, we briefly review the ORG algorithm (Yim et al., 1998) with only minor modifications as it is to be applied to projection angiography.

The ORG is an iterative region-growing process and is in the class of so-called dynamic programming algorithms. In this case, the ORG is applied to a discrete image, $I : D_I \to \boldsymbol{Z}$, whose domain is in the 2D plane, $D_I \subset \boldsymbol{Z}^2$. The algorithm is defined by four sets, R_n, B_n, G_n, and s_n all subsets of the image domain, D_I. R_n are the pixels within a growing region at iteration n. B_n are the pixels at the boundary of R_n. s_n and G_n are the seed point and growth points, respectively, at each iteration. The set of pixels adjacent to a given pixel, x, is designated N_x. Essentially, the region R_n grows outward at each iteration, but only to the pixels that are adjacent to a single point in its boundary, s_n, that is the point with the maximum intensity. Ultimately, the growth region, R_n, encompasses the entire image domain and thus does not function as a segmentation of the image as in conventional region-growing algorithms. However, the pattern of growth of R_n is meaningful, as it tends to reflect the directionality of small vessels in angiography. The growth pattern can be represented by an acyclic graph and construction of such a graph is the object of the ORG algorithm. The algorithm is iterative in nature and is defined more precisely as follows:

$$s_n = \{p \in B_n | \forall p' \in B_n, I(p) \geqslant I(p')\} \tag{1a}$$

$$G_n = N_{s_n} \setminus R_n \tag{1b}$$

$$R_{n+1} = R_n \cup G_n \tag{1c}$$

$$B_{n+1} = (B_n \cup G_n) \setminus s_n \tag{1d}$$

The "\" operator represents exclusion. The choice of the initial seed point s_0 is arbitrary. We chose s_0 to be at the center of the image. Furthermore, $R_0 = B_0 = s_0$. The algorithm proceeds until $G_n = \varnothing$ at which point the entire image is included in the growth region. The ORG graph is simply the pattern of growth and is described by the function Parent : $D_I \to D_I$. This function describes, for each point in the domain of the image, the point that annexed it to the growing region:

$$s_n = \text{Parent}(g), \quad \forall g \in G_n \tag{2}$$

Eight-neighbor adjacency is assumed although alternative adjacency may be equally valid. An example of the growth pattern of the ORG is shown in Fig. 1(a) and (b).

2.1. Trimming the acyclic graph

Vessel centerlines generally comprise the more "central" paths in the acyclic graph generated by the ORG algorithm. Therefore, a trimming process is an effective method for removing background points while preserving points on the vessel centerlines. The simplest possible trimming process would be the following iterative algorithm:

$$S_{m+1} = S_m \setminus T_m \tag{3}$$

where T_m is the set of terminal points and the initial skeleton, S_0, is the entire image domain, D_I. The terminal points can be defined as the set of points that are not upstream of any other point:

$$T_m = \{t \in S_m | \forall s \in S_m, t \neq \text{Parent}(s)\} \tag{4}$$

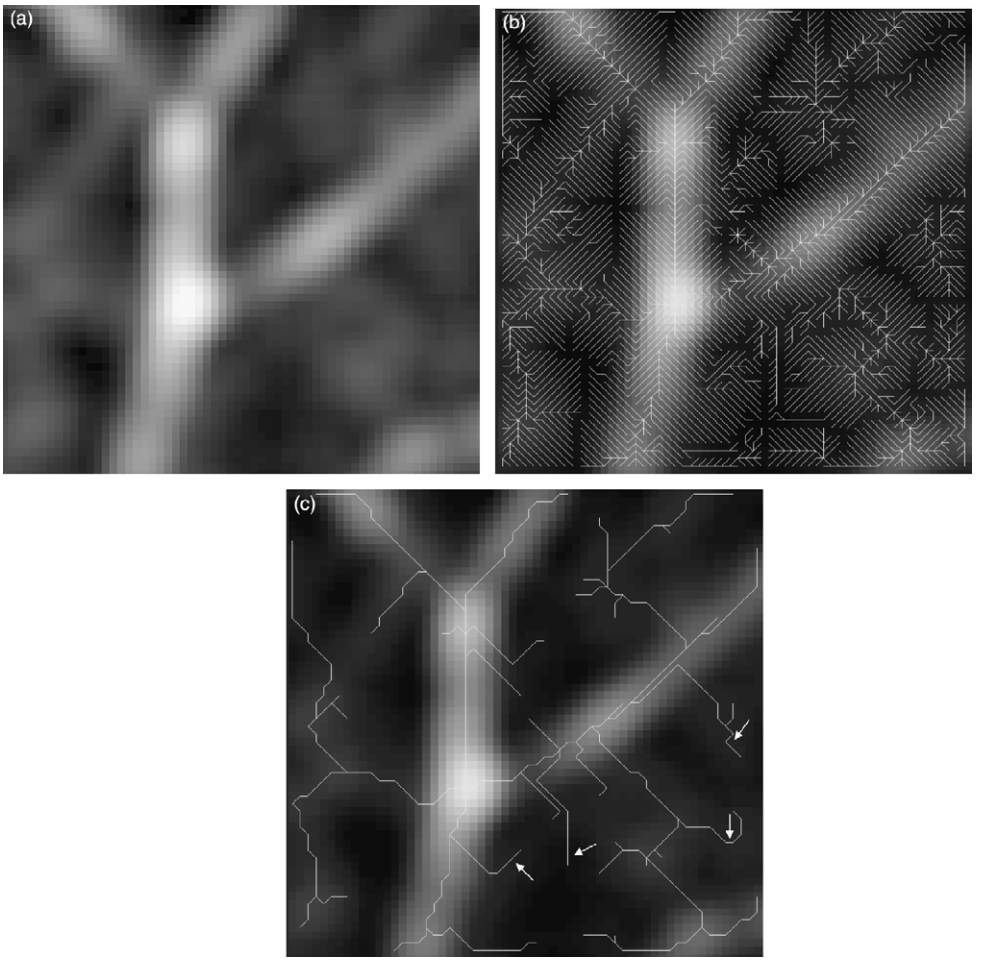

Fig. 1. The ORG algorithm generates a directed acyclic graph that spans the entire image. The ORG graph of an image is superimposed on the image in (b). The original image is shown in (a). Non-branching segments of the ORG graph are trimmed (three iterations) to obtain the central axis of the ORG graph (c). The detection of vessels by trimming of the ORG graph is overly inclusive; many of the branches in this result would not be considered, to be true vessels, by visual inspection. A few such spurious branches are indicated with arrows in bottom figure.

However, such an indiscriminant trimming process may require a considerable number of iterations to arrive at a meaningful skeletonization of the image. Thus, the trimming will have the undesirable effect of truncating the centerlines of some of the vessels. We propose an alternative trimming operation that minimizes any truncation of vessel centerlines. The trimming operation we propose is based on the observation that branches of the ORG graph that radiate outwards from the center of the vessels are largely non-branching, particularly when the ORG is applied to a blurred version of the image. In contrast, paths along the center of the vessels have a high degree of branching. This phenomenon is illustrated in Fig. 1(b). This trimming algorithm successively removes *segments* of the ORG graph, where a terminal segment, X_m^t is the set of points from a terminal point, t, up to but not including the nearest branch point. All terminal segments are removed according to the following iterative operation:

$$S_{m+1} = S_m \setminus X_m \tag{5}$$

Simply put, the set X_m is the union of all points in all terminal segments. To define this set more explicitly, some terminology has to be introduced. Firstly, a *bifurcation* is a point that has at least two downstream neighbors. The function, $\text{Downstream} : S_m \to Z$ describes the number of points that are downstream of any given point:

$$\text{Downstream}(s) = n(D_m^s) \tag{6}$$

where the set D_m^s is a set of points that are immediately downstream from a point s:

$$D_m^s = \{d \in S_m | s = \text{Parent}(d)\} \tag{7}$$

Thus, in those terms, the set of all bifurcation points at the mth trimming iteration is:

$$Y_m = \{s \in S_m | \text{Downstream}(s) \geqslant 2\} \tag{8}$$

Next, the concept of a terminal *segment* is defined. (The over-bar notation is used throughout the text to indicate an element or set that is a segment or is composed of *segments* of points.) There is a terminal segment, $\overline{X}_m^t$, that is associated with each terminal point t. The definition of a terminal segment is intuitive; it is simply the set of points from the terminal point up to, but not including, the closest bifurcation. Specifically:

$$\overline{X}_m^t = \bigcup_{i=1}^{k} p_i \tag{9}$$

where

$$p_1 \in T_m \tag{10a}$$

and

$$p_{i+1} = \text{Parent}(p_i) \quad \forall i \in [1, k-1] \tag{10b}$$

The upper limit, k of the index, i is such that no points in the segment are bifurcations:

$$p_i \notin Y_m \quad \forall i \in [2, k] \tag{11}$$

and the last point in the sequence, p_k is just below a bifurcation:

$$\text{Parent}(p_k) \in Y_m \tag{12}$$

Then the set $\overline{X}_m$ is the union of all terminal segments of the acyclic graph:

$$\overline{X}_m = \bigcup_{t \in T_m} \overline{X}_m^t \tag{13}$$

and the set of all *points* in all of the terminal segments is given by:

$$X_m = \bigcup_{\bar{x}_i \in \overline{X}_m} \{x \in \bar{x}_i\} \tag{14}$$

2.2. Statistical classification of segments

The trimming process described above produces a reduced acyclic graph (Fig. 1(c)) that is inclusive of nearly all vessel segments. Thus, the reduced acyclic graph provides a good set of paths that can be refined further with additional schemes. We propose a statistical model for further reduction or trimming of the acyclic graph. In this model, the reduced acyclic graph is evaluated segment-by-segment. A statistical comparison is made between the intensities along each segment of the graph and the intensities in the background. Presumably, for vessel segments, there is a statistically significant contrast between samples taken along the axis and with samples from the background. The appropriate statistical test for comparison of the intensities of two groups of pixels is the two-sample t-test. The t value for a given segment, $\bar{x}$, is obtained by (Woolson et al., 1987)

$$t(\bar{x}) = \frac{\bar{y}_1 - \bar{y}_2}{s_{\bar{y}_1 - \bar{y}_2}} \tag{15}$$

where $\bar{y}_1$ and $\bar{y}_2$ are the mean intensities along the axis of a given segment, $\bar{x}$, and in the background respectively. In this case, the null hypothesize of the t-test is that intensities along a given segment of the graph have the same average intensity as those in the background. The set of background points will be defined more precisely below but essentially includes non-vessel points. $s_{\bar{y}_1 - \bar{y}_2}$ is the sample standard error:

$$s_{\bar{y}_1 - \bar{y}_2} = \sqrt{\left(\frac{(n_1-1)s_1^2 + (n_2-1)s_2^2}{(n_1-1)+(n_2-1)}\right)\left(\frac{1}{n_1} + \frac{1}{n_2}\right)} \tag{16}$$

where n_1 and n_2 are the number of points sampled along the axis and in the background respectively. The sample variance of each group, s_i^2, is defined as follows:

$$s_i^2 = \sum_{j=1}^{n_i} \frac{(y_{ij} - \bar{y}_i)^2}{(n_i - 1)} \tag{17}$$

Given this statistical definition of the contrast of segments of the acyclic graph, a secondary trimming process can be defined that removes segments with low contrast. Segments are defined, as before, in terms of terminal points and bifurcations (10)–(12). Here, l is the iteration index. The set of segments with low contrast or a low t-value is:

$$\overline{X}_l^{\text{low}} = \{\bar{x} \in \overline{X}_l | t(\bar{x}) < 3.0\} \tag{18}$$

where the cutoff value of $t = 3.0$ was chosen based on trial-and-error. The set of all points to be removed consists of all points in all of those segments:

$$X_l^{\text{low}} = \bigcup_{\bar{x}_i \in \overline{X}_l^{\text{low}}} \{x \in \bar{x}_i\} \tag{19}$$

Those points are then removed in an iterative manner:

$$S_{l+1} = S_l \setminus X_l^{\text{low}} \tag{20}$$

This trimming process, based on image contrast, was carried out for five iterations. Initially, only terminal segments are evaluated as defined in (10)–(12). However, in the fifth and final iteration, segments of the graph between bifurcations are also evaluated and potentially removed. Thus, a modified definition of segments applies to the final iteration of trimming. In this iteration, the start point of a segment can be either a terminal point *or* a bifurcation. In contrast to (10a), the start points are:

$$p_1 \in T_l \cup Y_l \tag{21}$$

The background points are defined with respect to each given vessel segment. A scheme is proposed that minimizes the likelihood that the set of background points includes points on vessels. In this scheme, the background points are chosen along a line that is normal to the orientation of the segment and that passes through the center of the segment. Points on that line are excluded that are close to the segment, since the segment presumably passes along the center of the vessel. The line is placed through the midpoint of the segment where vessel directionality is unambiguous and where the line is most remote from adjacent vessel branches. The scheme is illustrated in Fig. 2.

The set of background points that is sampled for a given segment of the acyclic graph can be described in terms of the coordinates of the midpoint of the segment, $\bar{r}_j(p_{\text{mid}})$, and the orientation of the segment, $\bar{a}_j$. The directionality of the segment is defined in terms of the endpoints. For a segment with k points:

$$\bar{a}_j = \begin{cases} \bar{r}_j(p_k) - \bar{r}_j(p_1) & \text{if } k > 1 \\ \bar{r}_j(\text{Parent}(p_1)) - \bar{r}_j(p_1) & \text{if } k = 1 \end{cases} \tag{22}$$

The midpoint of the segment p_{mid} is point along the segment whose index is the midpoint between 1 and k.

$$\text{mid} = (k-1) \setminus 2 + 1 \tag{23}$$

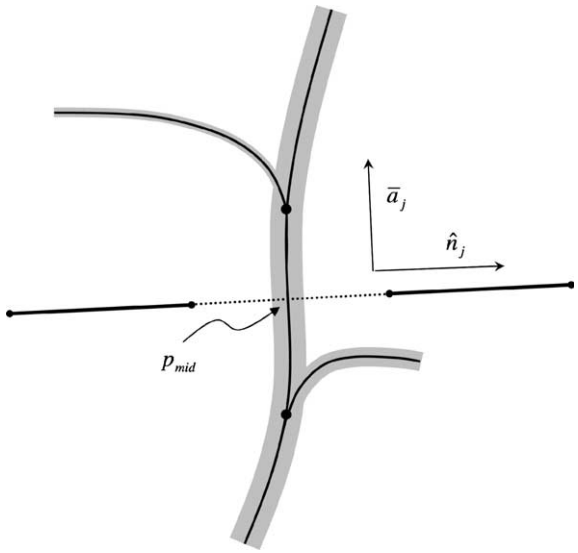

Fig. 2. Segments of the trimmed ORG graph are evaluated according to the statistics of the grey-scale intensities. The grey-scale intensities along each segment of the graph are compared with the off-axis intensities. Off-axis points are defined for each segment by a line that is in a direction, $\hat{n}_j$, that is perpendicular to the direction of the segment, $\bar{a}_j$, and passes through the midpoint of the segment, p_{mid}. Points along the off-axis line are not sampled near to the vessel segment (the dotted portion of the off-axis line).

Given the unit vector, $\hat{n}_j$ normal to the direction of the segment, $\bar{a}_j$, the coordinates of the sampled background points are:

$$N = \{-17\hat{n}_j + \bar{r}_j(p_{\text{mid}}), \\ -16\hat{n}_j + \bar{r}_j(p_{\text{mid}}), \ldots, \ldots -8\hat{n}_j + \bar{r}_j(p_{\text{mid}}), \\ 8\hat{n}_j + \bar{r}_j(p_{\text{mid}}), \ldots\ldots, 16\hat{n}_j + \bar{r}_j(p_{\text{mid}}), \\ 17\hat{n}_j + \bar{r}_j(p_{\text{mid}})\} \quad (24)$$

The intensities, y_{2j}, of the background points are obtained by bilinear interpolation and points outside of the domain of the image are excluded. The justification for choosing the points at 8–17 pixels from axis is somewhat arbitrary but reflects the observation that most of the vessels of interest in the image have a diameter of less than 16 pixels.

3. Application

The chick chorioallantoic membrane (CAM) assay is a promising assay for assessing the inhibition of vessel growth by novel anti-angiogenic drugs (Patan et al., 1997). Blood vessels can be visualized directly in the chick embryo's chorioallantoic membrane by confocal microscopy at optical resolutions. Contrast between vessels and the background tissue is enhanced by intravenous injection of a florescent contrast agent which provides exquisite detail of the vessels (Fig. 3(a)). Anitangiogenic effects are expected to occur mainly in the smaller vessels in the CAM assay. Thus, quantification must be accurate in that domain. Earlier studies of quantification of angiogenesis have suggested that total vessel length is a reasonable measure of vascularity (Merchant et al., 1994). Thus vessel centerlines, from which vessel length can be directly computed, are scientifically relevant. The result of the application of our detection algorithm on the CAM assay is shown in Fig. 3(b). For analysis of this image, the image was mildly blurred, prior to skeletonization, by convolution with a Gaussian with a space constant of $\sigma = 2$ pixels, which enhances the axis of all but the largest vessels. The vessels were also traced manually with Microsoft Paint. 75% of points of the skeletonization were within 6 pixels of a point within the manual tracing whereas 93% of points

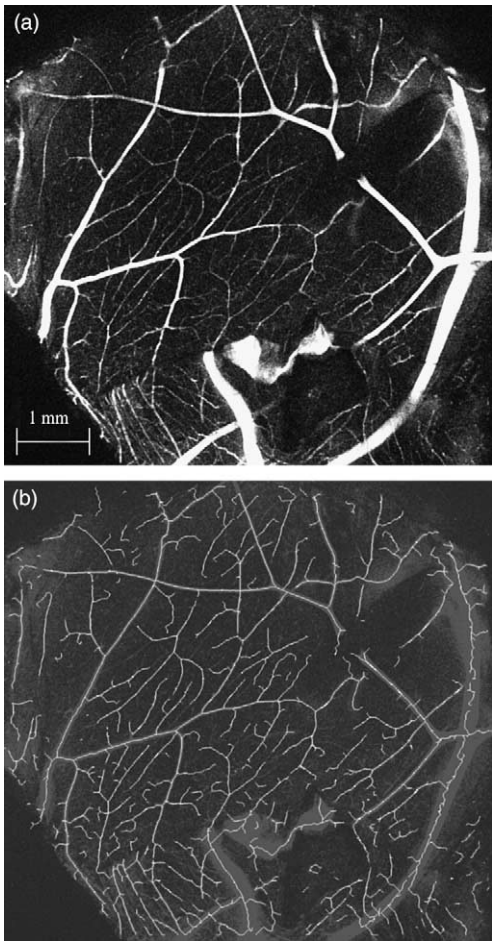

Fig. 3. Automated vessel detection is applied to confocal microscopic angiography of the CAM assay (a) for quantification of angiogenesis. Detected vessel segments are shown in (b). The angiogram is faintly displayed in the background for context.

on the manual tracing were within 6 pixels of a point on the skeletonization. The difference between results of the manual tracing and the skeletonization reflects, to a certain extent, the conservative approach taken in carrying out the manual tracing. The ORG algorithm was implemented in IRIS explorer (Numerical Algorithms Group, Oxford, UK) on an Octane. The trimming algorithms were implemented within IDL (Research Systems, Inc., Boulder, CO) on a PC. The entire skeletonization process is completed in less than 5 min.

4. Conclusions

The graph generated by the ORG algorithm is a powerful basis for vessel detection in a wide variety of angiography. Previously, we developed a semi-automated methodology based on the ORG algorithm for delineation of vessel paths in magnetic resonance angiography (Yim et al., 1998; Choyke et al., 2001). In this paper, a set of algorithms is presented that provides automated vessel detection in projection angiography by analysis of the ORG graph. The algorithms are quite straight-forward and incorporate natural features of vessel axes. These features include the high degree of branching along vessel axes in the ORG graph as well as the high contrast in image intensity between the on-axis and off-axis points. As it stands, the vessel detection scheme does not guarantee correct connectivity between vessel segments since the overlap of vessels can be misinterpreted as vessel branching. However, given the nearly complete set of vessel axes provided by these algorithms, the connectivity between segments can potentially be sorted out by consideration of vessel width, directionality, intensity and branching patterns.

References

Aylward, S.R., 2002. Initialization, noise, singularities, and scale in height ridge traversal for tubular object centerline extraction. IEEE Trans. Med. Imaging 21 (2), 61–75.

Brown, P.M., Zelt, D.T., Sobolev, B., 2003. The risk of rupture in untreated aneurysms: The impact of size, gender, and expansion rate. J. Vasc. Surg. 37 (2), 280–284.

Bullitt, E., Aylward, S., Bernard Jr., E.J., Gerig, G., 2001. Computer-assisted visualization of arteriovenous malformations on the home personal computer. Neurosurgery 48 (3), 576–582.

Choyke, P.L., Yim, P.J., Marcos, H., Mullick, R., Summers, R., Ho, V., 2001. Hepatic MR angiography: A multiobserver comparison of visualization methods. Amer. J. Roentgenol. 176, 465–470.

Cothren, R.M., Shekhar, R., Tuzcu, E.M., Nissen, S.E., Cornhill, J.F., Vince, D.G., 2000. Three-dimensional reconstruction of the coronary artery wall by image fusion of intravascular ultrasound and bi-plane angiography. Int. J. Card Imaging 16 (2), 69–85.

Eberly, D., Gardner, R., Morse, B., Pizer, S., Scharlach, C., 1994. Ridges for image analysis. J. Math. Imaging Vision 4 (4), 353–373.

Eichel, P.H., Delp, E.J., Koral, K., Buda, A.J, 1986. A method for fully automatic definition of coronary artery edges from cineangiograms. In: Proc. IEEE Comput. Cardiol., Boston, MA, p. 201.

Gering, D.T., Nabavi, A., Kikinis, R., Hata, N., O'Donnell, L.J., Grimson, W.E., Jolesz, F.A., Black, P.M., Wells 3rd, W.M., 2001. An integrated visualization system for surgical planning and guidance using image fusion and an open MR. J. Magn. Reson. Imaging 13 (6), 967–975.

Hazel, S.J., 2003. A novel early chorioallantoic membrane assay demonstrates quantitative and qualitative changes caused by antiangiogenic substances. J. Lab. Clin. Med. 141 (3), 217–228.

Merchant, F.A., Aggarwal, S.J., Diller, K.R., Bovik, A.C., 1994. In-vivo analysis of angiogenesis and revascularization of transplanted islets using confocal microscopy. J. Microsc. 176 (3), 262–275.

Merle, A.B., Finet, G., Lienard, J., Magnin, L.E., 1998. 3D reconstruction of the deformable coronary tree skeleton from two X-ray angiographic views. Comput. Cardiol. 25, 757–760.

Nguyen, T.V., Sklansky, J., 1986. Computing the skeleton of coronary arteries in cineangiograms. Comput. Biomed. Res. 19, 428–444.

Patan, S., Haenni, B., Burri, P.H., 1997. Implementation of intussusceptive microvascular growth in the chicken chorioallantoic membrane (CAM). Microvasc. Res. 53 (1), 33–52.

Rothwell, P.M., Gibson, R.J., Slattery, J., Warlow, C.P., 1994. Prognostic value and reproducibility of measurements of carotid stenosis. A comparison of three methods on 1001 angiograms. European Carotid Surgery Trialists' Collaborative Group. Stroke 25 (12), 2440–2444.

Sen, A., Lan, L., Doi, K., Hoffmann, K.R., 1999. Quantitative evaluation of vessel tracking techniques on coronary angiograms. Med. Phys. 26 (5), 698–708.

Sun, Y., 1989. Automated identification of vessel contours in coronary arteriograms by an adaptive tracking algorithm. IEEE Trans. Med. Imaging 8 (1), 78–87.

Woolson, R.F., 1987. Statistical Methods for the Analysis of Biomedical Data. John Wiley & Sons, New York.

Yim, P.J., Choyke, P.L., Summers, R.M., Kim, D., Lucas, C.L. The watershed and skeletonization of angiography, SPIE 2003 Med. Imaging, in press.

Yim, P.J., Kim, D., Lucas, C.L., 1998. High-resolution four-dimensional surface reconstruction of the right ventricle and pulmonary arteries. SPIE Proc. 3038, 726–738.

Yim, P.J., Summers, R.M., Choyke, P.L., 2000. Gray-scale skeletonization of small vessels in magnetic resonance angiograms. IEEE Trans. Med. Imaging 19 (6), 568–576.